RIGA TECHNICAL UNIVERSITY

Anzelms Zukuls

DEGENERATED ZNO NANOCRYSTALS: SYNTHESIS, PROPERTIES AND APPLICATIONS

Summary of the Doctoral Thesis

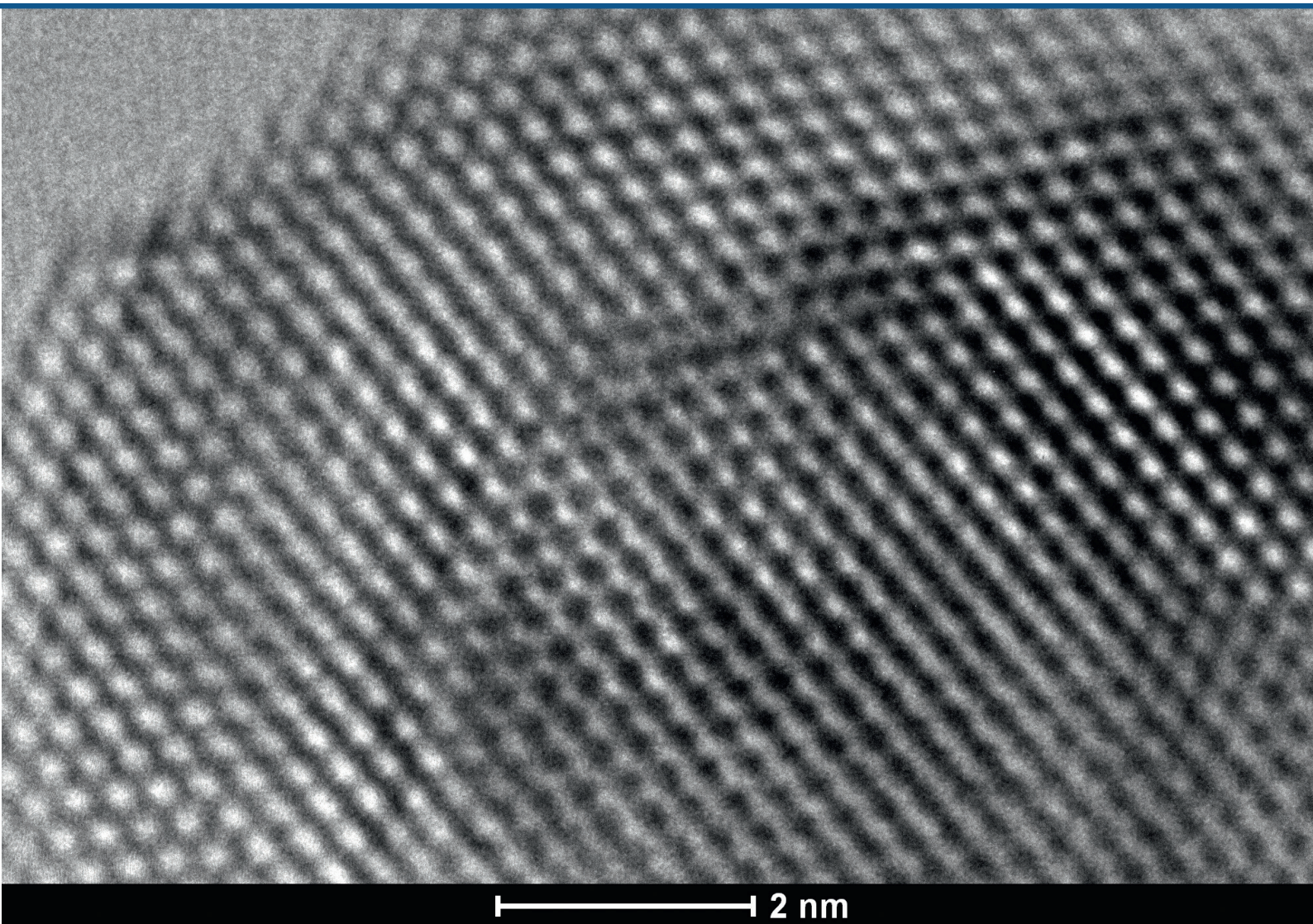

RTU Press
Riga 2021

RIGA TECHNICAL UNIVERSITY
Faculty of Materials Science and Applied Chemistry
Research Laboratory of Functional Materials Technologies

Anzelms Zukuls
Doctoral Student of the Study Programme "Chemical Technology"

DEGENERATED ZnO NANOCRYSTALS: SYNTHESIS, PROPERTIES AND APPLICATIONS

Summary of the Doctoral Thesis

Scientific supervisor
Associate Professor Dr. sc. ing.
ANDRIS ŠUTKA

RTU Press
Riga 2021

Zukuls, A. Degenerated ZnO Nanocrystals: Synthesis, Properties and Applications. Summary of the Doctoral Thesis. Riga: RTU Press, 2021. 32 p.

Published in accordance with the decision of promotion council "RTU P-01" of 29–30 April 2020, Nr. 04030-9.1/2.

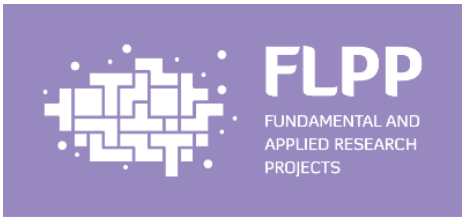

This work was developed within the framework of FLPP projects of the Latvian Council of Science (Plasmonic Oxide Quantum Dots for Energy Saving Smart Windows, lzp-2018/1-0187).

https://doi.org/10.7250/9789934225871
ISBN 978-9934-22-586-4 (print)
ISBN 978-9934-22-587-1 (pdf)

DOCTORAL THESIS PROPOSED TO RIGA TECHNICAL UNIVERSITY FOR THE PROMOTION TO THE SCIENTIFIC DEGREE OF DOCTOR OF SCIENCE

To be granted the scientific degree of Doctor of Science (*Ph. D.*), the present Doctoral Thesis has been submitted for the defence at the open meeting of RTU Promotion Council on February 18 2021 at 14:00 online. https://rtucloud1.zoom.us/j/9352086644.

OFFICIAL REVIEWERS

Asoc. Profesor Dr. sc. habil. ing. Visvaldis Švinka
Riga Technical University, Latvia

Leading researcher Ph. D. Donāts Erts
University of Latvia, Latvia

Researcher Dr. Phys. Irēna Mihailova
Daugavpils University, Latvia

DECLARATION OF ACADEMIC INTEGRITY

I hereby declare that the Doctoral Thesis submitted for the review to Riga Technical University for the promotion to the scientific degree of Doctor of Science (Ph. D.) is my own. I confirm that this Doctoral Thesis had not been submitted to any other university for the promotion to a scientific degree.

Anzelms Zukuls ……. (signature)

Date: ……

The Doctoral Thesis has been written in Latvian. It consists of an Introduction; 3 chapters; Conclusions; 83 figures; 20 tables; the total number of pages is 111. The Bibliography contains 160 cited literature sources.

ACKNOWLEDGEMENTS

I would like to express my gratitude to everyone who directly or indirectly helped me with my Doctoral Thesis and provided moral support during this time.

I am grateful to the scientific supervisor of my Doctoral Thesis, Andris Šutka, for giving me this second chance in science, to grow and improve myself as a young researcher and to work in a lab with highly determined and motivated colleagues.

I would like to express my warm and sincere thanks to all my excellent and responsive colleagues in the Research Laboratory of Functional Materials Technologies, especially Raivis Eglītis and Kaspars Mālnieks, for their support in my day-to-day work and for tips regarding my Doctoral Thesis.

Thanks to RTU Institute of Technical Physics for giving me the opportunity to measure optical properties. Also, thanks to the Optical Materials Laboratory of the Institute of Solid State Physics, University of Latvia, and to Krišjānis Šmits for the photoluminescence measurements and TEM images, and many thanks to the Institute of Physics, University of Tartu, and Swiss Federal Institute of Technology in Lausanne for taking various measurements during the development of my work. Thanks to Māra Plotniece for help in the final steps of the dissertation.

This job would not have been done so quickly without the support and help of my girlfriend Ramona, who did not allow me to give up and stayed up late together with me. As promised, we now can bake pizzas and get feather spices in all of our food by adopting a lovely and fluffy cat.

I would also like to thank my family – my mom Marija, father Dainis and brother Artis – for being with me, for the given wisdom, and for inspiring me to continue my master's and doctoral studies.

CONTENTS

General Overview of the Doctoral Thesis 6
Current Solutions and Problems in the Field 6
Aprobation 8
Literature Review 10
Materials and Methods 12
Results and Discussion 13
1. Characterisation of Gallium Doped ZnO 13
2. Influence of the Synthesis Medium on the Properties of GZO Nanocrystals 16
3. Control of ZnO Charge Carriers by Photodoping 20
4. Transition Metal and Transition Metal-Gallium Co-Doped ZnO Diluted Magnetic Semiconductors 24
Conclusions 30
References 31

GENERAL OVERVIEW OF THE DOCTORAL THESIS

Current Solutions and Problems in the Field

Zinc oxide has attracted the attention of scientists for a long time. Its wide availability and combination of good chemical and physical properties have made it a suitable candidate for the development of semiconductor devices. By doping it with aliovalent dopants, it is possible to modify the ZnO zone structure of it and adapt the properties of the newly obtained material according to their requirements. By introducing gallium, aluminium, etc. into the zinc oxide structure, it is possible to obtain metal oxides with degenerated semiconductor properties. The conductivity of these oxides is similar to that of metals, and their application offers ample opportunities for the development of new innovative materials or devices (smart windows, sensors, etc.). Direct light transmission and high conductivity are what modern smart devices are based on – phone screens, touch screens, etc., so the development of these materials is important for the growth of electronic devices. The conductivity of degenerated metals oxides is not as high as that of metals. Scientists are seeking pathways to improve the electric conductivity. The concentration of free charge carriers in degenerated ZnO can be adjusted by controlling the type and amount of dopants or point defects. This also provides a function to modulate infrared light absorption for ZnO plasmonic nanoparticles. Switchable or passive infrared absorption in these materials is especially important for smart window devices for energy management in buildings.

The concentration of free charge carriers in metal oxide semiconductor materials can be increased by using photodoping. In this process, nanoparticle suspensions are dispersed in various photogenerated hole scavenger mediums (ethanol, butanol, etc.) that act as hole scavengers. Under the influence of ultraviolet light or other light radiation (where the radiation energy is greater than the width of the band gap of the semiconductor material) hole and free electron pairs are created. In the presence of alcohols, the photogenerated holes are removed, causing free electrons to accumulate in the conduction or valence zone. Unfortunately, so far this method has not made it possible to obtain nanoparticles with a permanent photodoping effect. Under normal conditions, photodoped nanoparticles lose the accumulated free electrons when exposed to air or other oxidizing substances, leading to a decrease in delocalized electron concentration. In our work, we demonstrate for the first time in which cases photodoping in the ambient air is possible.

Free charge carriers are also important for the modulation of magnetic properties in ZnO-based diluted magnetic semiconductors. It is well known that by doping zinc oxide with magnetic ions (such as cobalt, nickel, chromium, manganese, iron, etc.), it is possible to obtain dilute magnetic semiconductor oxides in which delocalized valence zone or conduction zone charge carriers interact with the magnetic dopant in the zinc oxide material localized spin. By adjusting the dopant and its amount, it is possible to change the magneto-optical and magneto-electrical properties of the material. The weak ferromagnetic interactions that can be obtained from these materials allow them to be used in the design of electrical devices and storage media. Considering that the localized spin of magnetic ions interacts with the free

charge carriers of the conduction zone, it is hypothesized that by changing the concentration of free electrons in the structure of zinc oxide band structure, it is possible to change/adjust the magnetic properties of the obtained nanoparticles. For this reason, the synthesis of zinc oxide nanoparticles doped with transition metals and Ga^{3+} ions is performed. Gallium ion acts as an element of the donor group, creating additional free electrons in the conduction zone, which would improve magnetic spin interaction. It is unequivocally that modifying the structure of zinc oxide with gallium and/or a transition metal also changes the optical and magnetic properties of the obtained sample. Changes in the concentration of free charge carriers by photodoping are most pronounced as an increase in absorption in the infrared region of the spectrum, which indicates additional possibilities to obtain materials with their desired properties.

Aims of the Doctoral Thesis

To obtain degenerate ZnO nanocrystals with high concentration of free electrons and light absorption in the infrared part of the spectrum, as well to study the effect of their free charge carriers on the magnetic properties of ZnO doped with transition metal (Fe^{3+}, Ni^{2+} or Mn^{2+}).

Tasks of the Doctoral Thesis to Complete the Proposed Aims

- To carry out synthesis and Ga^{3+} doping of ZnO nanocrystals using the solvothermal synthesis method in different synthesis media.
- To investigate the crystalline, electronic and optical properties of synthesized ZnO materials.
- To study the effect of photodoping on the optical properties of the synthesized Ga^{3+} doped ZnO.
- To formulate the conditions for the formation of free charge carriers in Ga^{3+} doped ZnO.

Scientific Significance and Novelty of the Doctoral Thesis

The conditions for the formation of free charge carriers and their influence on the optical and magnetic properties in ZnO nanocrystals synthesized by the solvothermal method have been formulated.

Practical Significance

Doped ZnO nanocrystalline materials with tuneable optical properties could provide applications in smart windows with switchable infrared absorption for energy management in buildings. Materials can be used as well for electronics, conductive transparent coatings, sensor materials, various optical materials, and more. Their application depends on the chemical and physical properties, which in turn depend on the concentration and position of the donor in the lattice, the presence and concentration of other point defects, and the size and shape of the nanocrystals.

Thesis Statements to Be Defended

1. At fixed metal Ga: Zn salt ratios under reducing synthesis medium conditions, it is possible to obtain Ga-ZnO nanoparticles with a higher degree of doping using the solvothermal synthesis method.
2. Irradiation of Ga-ZnO nanocrystalline dispersions with UV light in the environment of photogenerated hole scavengers can permanently increase the concentration of free electrons in materials.
3. In diluted magnetic oxide semiconductor nanocrystals, the magnetic properties can be adjusted by changing the point defect concentration.

Approbation of the Results

The scientific results of the research within this Doctoral Thesis have been summarised in 3 scientific articles and presented at 4 international conferences.

Aprobation

Publications

1. Šutka, A., Zukuls, A., Eglītis, R., Kaambre, T., Kook, M., Vlassov, S., Rubenis, K., Ignatāns, R. Stronger Reductive Environment in Solvothermal Synthesis Leads to Improved Ga Doping Efficiency in ZnO Nanocrystals and Enhanced Plasmonic Absorption. Physica Status Solidi A: Applications and Materials Science, 2019, Vol. 216, No. 22, pp. 1900335–1900335. e-ISSN 1862-6319. Available: doi:10.1002/pssa.201900335
2. Zukuls, A., Eglītis, R., Kaambre, T., Kook, M., Kisand, V., Maiorov, M., Ignatāns, R., Duarte, R., Järvekülg, M., Šutka, A. Magnetic and Optical Properties in Degenerated Transition Metal and Ga Co-substituted ZnO Nanocrystals. Journal of Alloys and Compounds, 2019, Vol. 805, pp. 1191–1199. ISSN 0925-8388. Available: doi:10.1016/j.jallcom.2019.07.197
3. A. Zukuls, R. Eglītis, T. Käämbre, R. Ignatans, K. Šmits, K. Rubenis, D. Začs, A. Šutka. Permanent photodoping of plasmonic gallium-ZnO nanocrystals. Nanoscale. 2020, 12, 6624–6629, Available: doi.org/10.1039/D0NR01005G

Patents

P-19-57 Andris Šutka, Anzelms Zukuls, Raivis Eglītis. Method for increasing the electrical conductivity of degenerate oxide semiconductors. Submitted: 06.11.2019.

Presentations at Conferences

1. Seņko, M., Bite, I., Zukuls, A., Spustaka, A., Roze, K., Šmits, K., Grigorjeva, L. Inactivated and activated synthesis of ZnO nanoparticles and investigation of their properties. Unveristy of Latvia, Institute of Solid State Physics, 35th Scientific Conference, Riga, Latvia, 22–24 February 2019.

2. Eglītis, R., Šutka, A., Zukuls, A., Viter, R. A Study of the TiO_2 Photochromic Response Kinetics in Different Solvents. 6th Nano Today Conference: Book of Abstracts, Portugal, Lisbon, 16–20 June 2019.
3. Zukuls, A., Šutka, A. Permanent photodoping of ZnO nanoparticles. No: Particle Based Materials Symposium 2019: Conference Thesis, Germany, Ulm, 26–27 September 2019.
4. Eglītis, R., Šutka, A., Zukuls, A., Viter, R. Photochromic Properties of TiO_2. 60th International Scientific Conference Materials Science and Applied Chemistry: Book of Abstracts, Latvia, Riga, 24–24 October 2019.
5. Dūrena, R., Bite, I., Spustaka, A., Zukuls, A. Synthesis of inactivated and Li-activated ZnO and comparison of their properties. University of Latvia, Institute of Solid State Physics, 36th Scientific Conference, Riga, Latvia, 11–13 February 2020.
6. Zukuls, A., Šutka, A., Eglītis, R. Permanent photodoping of Ga doped ZnO nanoparticles. 16th Zsigmondy colloquium - Soft Colloids, Germany, Dusseldorf, 9–11 March 2020.
7. Eglītis, R., Šutka, A., Zukuls, A. Synthesis and photochromic properties of Nb-doped TiO_2 colloidal nanoparticles. 16th Zsigmondy colloquium – Soft Colloids, Germany, Dusseldorf, 9–11 March 2020.

LITERATURE REVIEW

Modification of semiconductor oxides with both acceptor/donor group elements and transition metals provides new materials with desired properties for many research fields and applications. Metal oxide nanocrystals, which have high plasmon absorption in the infrared spectral region and low light absorption in the visible spectral region, are particularly important for the development of smart window technologies for building energy management. The absorption of infrared light in oxide semiconductors depends to a large extent on the amount of free electrons in the conduction band. By controlling the free electron concentration, it is possible to adjust the infrared absorption [1]. Great efforts are being made to increase the concentration of charge carriers in the degenerate semiconductor materials. Higher delocalized electron concentrations would lead to higher electric conductivity and infrared absorption. Diluted magnetic semiconductor materials also benefit from delocalized charge carriers due to enhanced magnetic spin interactions. This is important for designing spintronic devices [2].

Unlike metal plasmonic nanoparticles where optical properties are only size dependent, the plasmonic resonance in degenerated semiconductors can be additionally controlled or even switched on/off by changing the type and degree of doping as well as the dopant distribution in the nanocrystal. This ability to adjust light absorption stimulates interest in metal oxide nanocrystals and their applications in chemical sensors and biosensors, telecommunications, optics and photonics [3]–[5].

In the literature review of the work, a lot of attention is paid to the methods of ZnO nanocrystal synthesis. All the methods included in the literature review can be divided into three groups: (1) physical methods (high energy bullet milling, pulsed laser application, laser pyrolysis, flame spray pyrolysis, electrospray); (2) biological methods (microorganism-assisted biogenesis); (3) chemical methods (sol-gel synthesis, microemulsion technique, hydro-/solvo-thermal synthesis, polyol synthesis, chemical vapor synthesis). The variety of products obtained in these syntheses is striking. Each of these methods is unique in its own way, which makes them specific for obtaining certain products. One of the most common methods in the synthesis of ZnO nanocrystals is the solvothermal (hydrothermal, if the synthesis medium is water) method. Its advantage is the ability to obtain powdered metal oxide nanocrystals with controlled properties, which can be obtained by changing the pressure, temperature and properties of the supercritical or near-supercritical solvent [6].

In metal oxide semiconductors, at low dopant concentrations, free charge carriers are localized at discrete impurity levels, but at sufficiently high concentrations, charge carriers are localized to form of a donor/acceptor bonds rather than discrete energy levels. The formation of free charge carriers in materials is achieved by performing: (1) internal doping – creating lattice vacancies; (2) external aliovalent substitution doping; and (3) external interstitial doping. To obtain degenerate oxide, the charge imbalance from dopant must be compensated with an electron or hole not other point defects such as cation/anion

vacancies or interstitials. This dynamic balance between defect activation and compensation as a result of oxidation and reduction determines the properties of free electrons [7].

Photochemical charging or photodoping has become an alternative method for dynamic modulation of electron density in semiconductor oxides. UV irradiation leads to the accumulation of electrons in the conduction band on the semiconductor oxide. However, by exposing the photodoped material to an oxidizer (air), the electrons accumulated in the conduction band are diminished, which returns the material to its original state [7], [8].

MATERIALS AND METHODS

In this work sample synthesis is done by the using solvothermal synthesis method, which is schematically depicted in Fig. 1. After solvothermal synthesis, when the pressure vessel has cooled down, the resulting particles and solution are centrifuged, decanted and washed with methanol and centrifugation three times. The resulting particles are dried at room temperature in an air atmosphere.

The performed research can be divided into 4 parts. The first part involves the synthesis of ZnO nanocrystals doped with different gallium contents in methanol and the study of their properties.

In the second part, gallium-doped ZnO is synthesized with a fixed ion ratio in different synthesis solution media. During these studies, the effect of solvent environment and various reducing agents on the concentration of delocalized electrons is determined.

In the third part, these properties are modified by photodoping. These particles are subjected to photodoping studies during which dispersions of particles in the presence of hole scavengers are treated in ultraviolet light. The samples are placed in closed glass bottles with Teflon septic gasket.

In the fourth part, ZnO nanoparticles are doped with a transition metal (Me = Mn, Fe or Ni) as well as gallium at a fixed amount of Me ions. The introduction of transition metals into the ZnO crystal lattice is performed to obtain diluted magnetic semiconductors. The introduction of gallium into these materials is based on the fact that their presence could promote the formation of delocalized electrons, which would lead to improved magnetic properties.

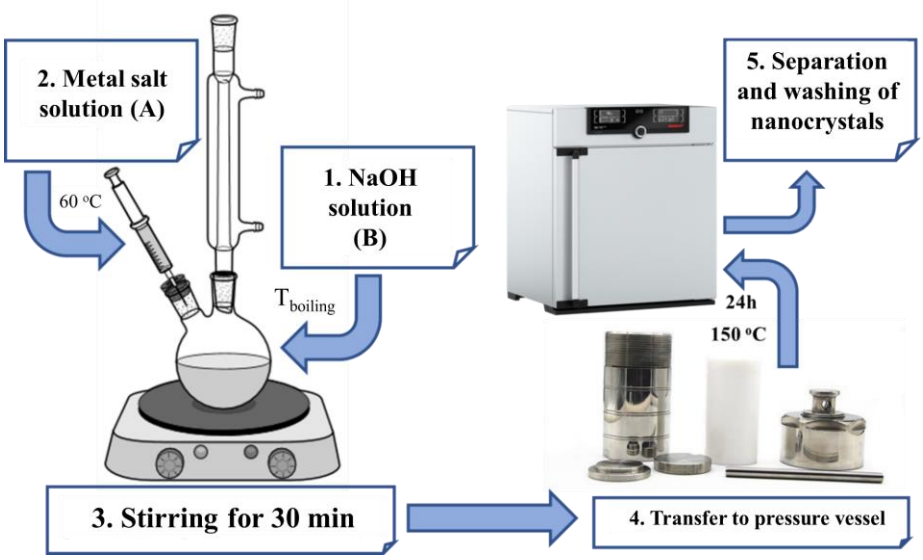

Fig. 1. Schematic diagram of synthesis process and equipment.

RESULTS AND DISCUSSION

1. Characterisation of Gallium Doped ZnO

The following subsection is presenting the properties of gallium doped ZnO (GZO) materials synthesized in methanol. Figure 2 shows the X-ray diffraction patterns of ZnO powders doped with various gallium contents. Gallium content in ZnO was 0 mol %; 2.5 mol %; 5.0 mol %; 7.5 mol %; 10 mol %; 15 mol %; 20 mol %; 25 mol % and 30 mol %. The obtained X-ray diffraction patterns correspond to the crystalline phase of ZnO (JCPDS 36-1451) wurtzite with symmetry group P63mc. Corresponding lattice parameters at 2θ = 31.8° (100), 34.5° (002), 36.3° (101), 47.6° (102), 56.6° (110), 62.9 (103), 68.0 (112) and 69.1 (201). Figure 2 shows that as the gallium content in the ZnO nanocrystals increases, crystallite and particle size decreases are observed, as evidenced by the decrease in peak height and increase in width. These peak shape changes are due to the decrease of nanocrystal sizes and the formation of defects in the ZnO crystal lattice by the presence of gallium ions.

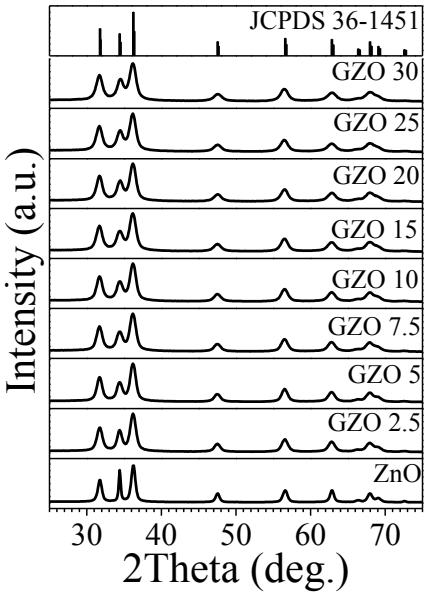

Fig. 2. X-ray diffraction patterns of ZnO samples doped with various gallium contents.

A summary of the Rietveld calculations and X-ray photoelectron spectroscopy results is shown in Table 1. As can be seen from the crystallite size calculations, the introduction of gallium into the system reduces the particle size in *a* and *b* (100 and 010), and *c* (001) axes. In addition, the formation of microstrain is observed as the amount of gallium increases. X-ray photoelectron spectroscopy results show that Ga^{3+} ions are present in the obtained nanopowders. When increasing the degree of doping, the doping efficiency gradually decreases from 80 % with 2.5 mol % gallium doped ZnO to just 23.33 % with 30 mol % gallium doped ZnO. Figure 3 (a)–(c) clearly shows the effect of increasing gallium content on the parameters of the crystal lattice. As the lattice parameter *a* and *b* increase and lattice parameter *c* decreases, the resulting cell volume ($Å^3$) increases.

Table 1

Summary of the Rietveld Refinement and X-Ray Photoelectron Spectroscopy Calculations of ZnO Samples Doped With Various Gallium Contents

Nominal Ga amount, mol %	Crystallite sizes		Micro strains $\sqrt{k2}$	Metal ion ratio		Doping efficiency, %
	***d*(100), nm**	***d*(001), nm**		**Ga, %**	**Zn, %**	
0	19.96 ± 0.16	69.80 ± 1.50	0.0024	–	100.0	–
2.5	14.72 ± 0.13	23.96 ± 0.33	0.0049	2.0	98.0	80.00
5.0	15.08 ± 0.13	21.01 ± 0.26	0.0050	3.5	96.5	70.00
7.5	14.30 ± 0.14	19.87 ± 0.27	0.0060	3.8	96.2	50.67
10	14.33 ± 0.14	19.80 ± 0.28	0.0063	4.4	95.6	44.00
15	13.25 ± 0.13	18.00 ± 0.25	0.0066	5.4	94.6	36.00
20	14.49 ± 0.16	20.30 ± 0.32	0.0077	5.7	94.3	28.50
25	14.65 ± 0.19	20.73 ± 0.40	0.0089	6.7	93.3	26.80
30	13.52 ± 0.16	19.60 ± 0.35	0.0087	7.0	93.0	23.33

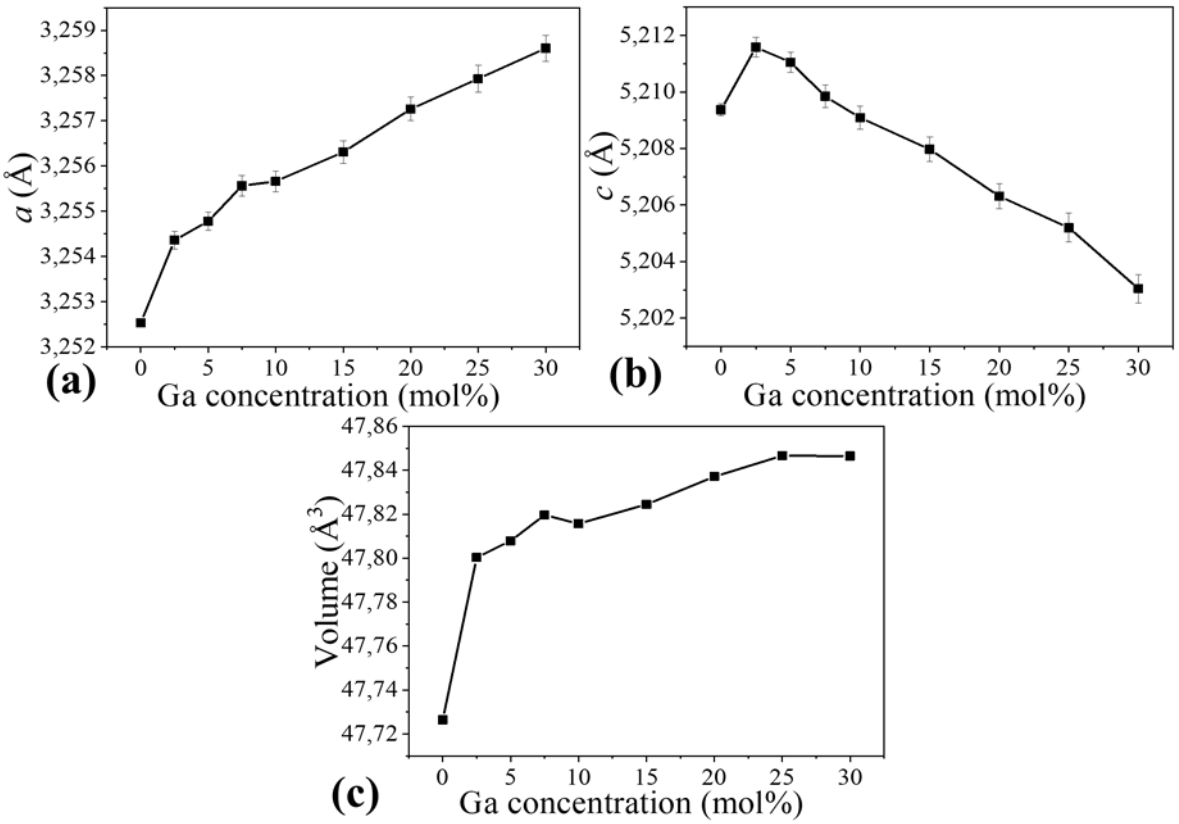

Fig. 3. The change of lattice parameters in ZnO by increasing the content of Ga^{3+} ions in (a) *a* axis direction, (b) in the *c* axis direction and (c) change in the primitive unit cell volume.

Transmission electron microscopy images are shown in Fig. 4. As can be seen from the figures, the size of ZnO particles synthesized in methanol decreases with the increasing amount of gallium in the obtained samples. A decrease in the crystal size confirms observations on X-ray diffraction patterns. As shown, pure ZnO nanocrystals have a diameter

of about 20 nm and a length of up to 50 nm. As the amount of Ga^{3+} ions increases, the particle size decreases to about 10–20 nm.

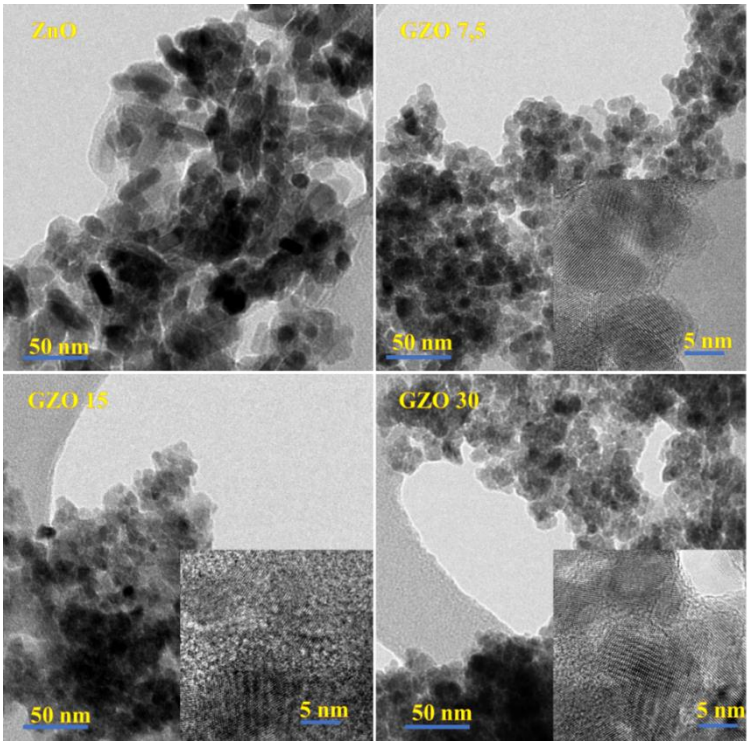

Fig. 4. Transmission electron microscopy images of ZnO and Ga doped samples.

The change in the amount of gallium in the samples can be seen from the Ga 2p binding energy lines (Fig. 5) obtained at the same Zn 2p intensity values. It can be observed that increasing the amount of gallium in ZnO nanocrystals also increases the intensity of Ga 2p binding energy lines.

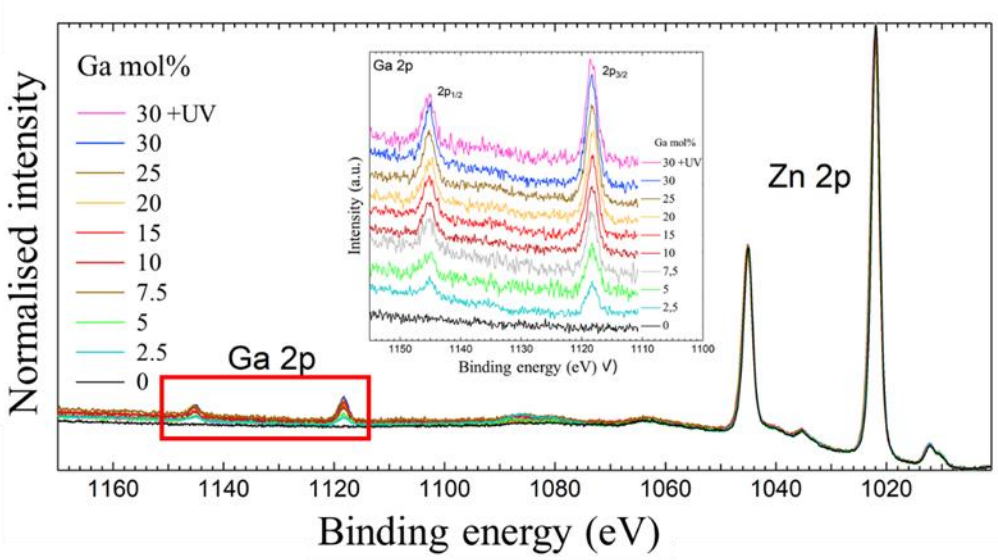

Fig. 5. Ga 2p hard X-ray photoelectron spectroscopy spectra of various Ga doped ZnO samples normalized at the same Zn 2p intensity values.

2. Influence of the Synthesis Medium on the Properties of GZO Nanocrystals

In the same method, gallium-doped zinc oxide nanocrystals in various solvents and additives were obtained. Methanol, ethanol and mixtures of ethanol-butanol, ethanol-$NaBH_4$ and ethanol-butanal (butyraldehyde) were used. The amount of gallium in this system was fixed to a certain amount – 10 mol %.

The results of X-ray diffraction patterns of these obtained samples show formation of a wurtzite crystalline phase corresponding to the JCPDS 36-1451 crystalline structure of ZnO (Fig. 6 (a)). ATR-FTIR spectra were also obtained to confirm their purity from organic impurities (Fig. 6 (b)). As can be seen from the obtained results, no peaks of organic groups can be observed in the spectra confirming the purity of the samples. At 1450 cm^{-1}, characteristic oscillations of the Zn-OH group are observed, where -OH groups are formed on the surface of ZnO nanoparticles.

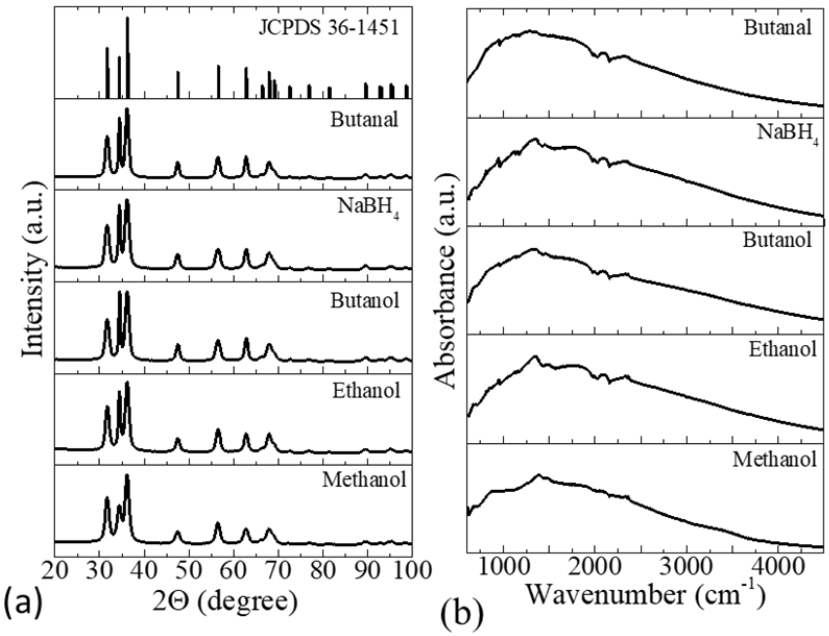

Fig. 6. (a) X-ray diffraction patterns and (b) ATR-FTIR measurement results of $Zn_{0.9}Ga_{0.1}O$ samples synthesized in various solvents.

The scanning electron microscopy (SEM) results are summarized in Fig. 7 (a)–(e). In addition to these SEM images, a visual image of the synthesis nanopowders is attached. As it can be seen from the SEM images, these particles have a size of about 15 nm. Also, the particle size distribution is very similar throughout the sample volume. These nanopowders exhibit a distinct shade ranging from yellow to grey-blue.

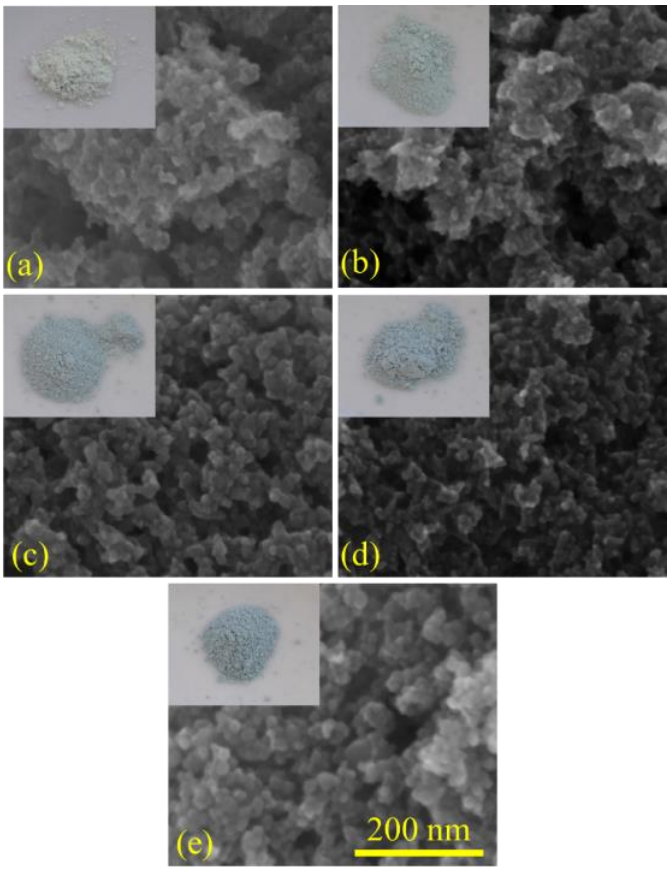

Fig. 7. Scanning electron microscopy results for $Zn_{0.9}Ga_{0.1}O$ systems obtained in various media: (a) methanol, (b) ethanol, (c) butanol, (d) $NaBH_4$, and (e) butanal.

From the normalized spectra of Ga 2p (Fig. 8 (a)) at 1118 eV (Ga $2p_{3/2}$) and 1145 eV (Ga $2p_{1/2}$), it can be seen that $Zn_{0.9}Ga_{0.1}O$ nanocrystals synthesized in different media have different Ga^{3+} ion content. This indicates that the efficiency of the synthesis can be controlled by changing the environment to facilitate the doping processes. Looking at Fig. 8 (b), which shows the same hard X-ray photoelectron spectroscopy spectrum but for a deeper penetration depth, it can be concluded that gallium is also inside the nanoparticles, indicating that Ga^{3+} ions have been scattered throughout the ZnO nanoparticle volume.

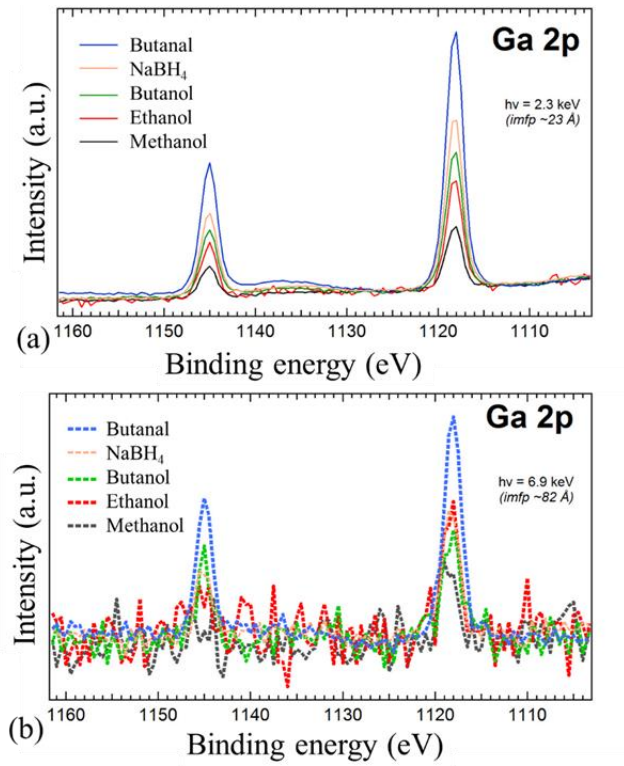

Fig. 8. Hard X-ray photoelectron spectroscopy results for Ga 2p peaks obtained from samples of $Zn_{0.9}Ga_{0.1}O$ nanocrystals synthesized in different media (normalized to the same Zn 2p height), (a) at 2.3 keV (mean free path length of inelastic electrons 23 Å) and (b) at 6.9 keV (mean free path length of inelastic electrons 82 Å).

The optical absorption spectra of $Zn_{0.9}Ga_{0.1}O$ obtained in different solvents are shown in Fig. 9. As can be seen, all gallium doped samples exhibit plasmon resonance absorption in infrared spectrum. The presence of free electrons in the conductivity zone causes the observed absorption, which is due to the formation of free electrons caused by zinc substitution with gallium. This substitution results in formation of free electrons, which forms electron neutrality of lattice according to following equation:

$$Ga_2O_3 \rightarrow 2Ga_{Zn}^{\bullet} + 2e^{-} + 2O_O^X + \frac{1}{2}O_2 \uparrow . \quad (1)$$

An increase in infrared absorption of $Zn_{0.9}Ga_{0.1}O$ samples synthesized in various media is observed in the following order: methanol < ethanol < butanol. Samples supplemented with $NaBH_4$ and butanal show higher absorption in infrared spectrum. The different effects of alcohols and their additives can be explained by the fact that the synthesis medium may have different reducing properties. To prove this, $NaBH_4$ and butanal, which are strong reducing agents, were added during the synthesis. Given the chemical equation of defect (1), it is seen that in order to improve the substitution potential of gallium, it is necessary to efficiently collect excess oxygen from the synthesis medium. In this case, judging by the results, more reducing conditions of the synthesis environment can ensure more successful substitution of gallium in the ZnO crystal lattice.

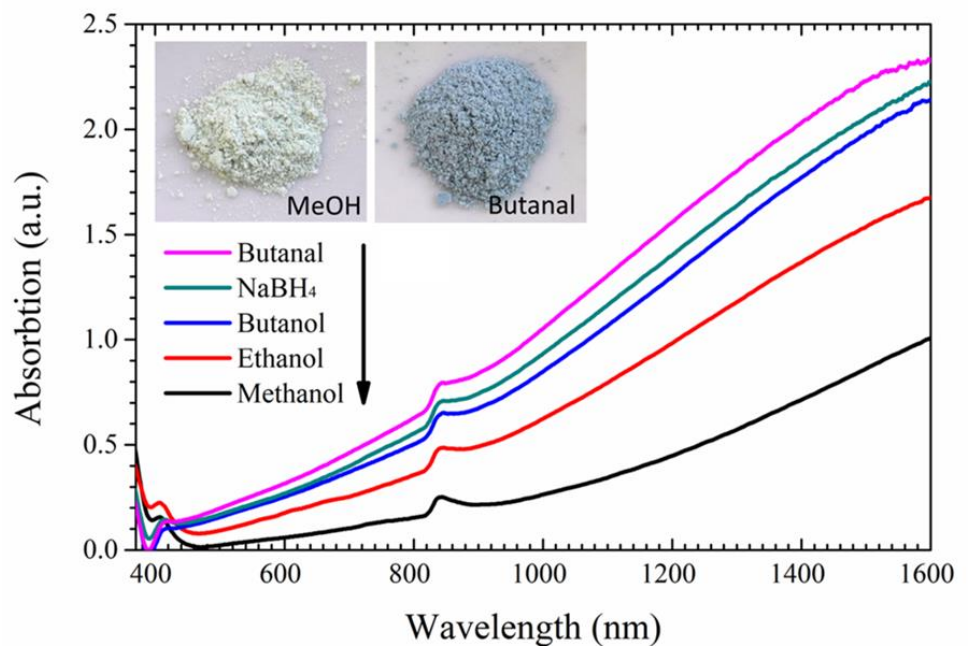

Fig. 9. Optical absorption spectrum for $Zn_{0.9}Ga_{0.1}O$ nanoparticles obtained in various synthesis media.

Table 2

Summary of Rietveld Refinement and Other Determined Parameters

Parameters	**Methanol**	**Ethanol**	**Butanol**	**$NaBH_4$**	**Butanal**
***a*, Å**	3.25607	3.2568	3.25887	3.25783	3.25818
Δ*a*, Å	±0.00048	±0.00041	±0.00044	±0.00049	±0.00036
***c*, Å**	5.21024	5.20992	5.20462	5.20591	5.20729
Δ*c*, Å	±0.00085	±0.00073	±0.00077	±0.00085	±0.00066
c*/*a	1.600	1.600	1.597	1.598	1.598
Crystallite sizes (100), nm	13.02 ± 0.27	12.44 ± 0.21	12.35 ± 0.22	12.14 ± 0.23	14.62 ± 0.26
Crystallite sizes (001), nm	16.27 ± 0.44	31.70 ± 1.30	62.90 ± 6.00	45.30 ± 3.20	54.80 ± 3.90
***V*, $Å^3$**	47.84	47.86	47.87	47.85	47.87
Doping amount, %	2.06	3.61	3.64	4.54	7.14
Doping efficiency, %	20.6	36.1	36.4	45.4	71.4
Band gap, eV	3.24	3.25	3.29	3.31	3.32

Table 2 shows the results of the Rietveld refinement and other calculations. From these results it can be concluded that by changing alcohols it is possible to change the dimensions of *a* and *b* unit cells in the direction of crystallographic axes – the distance of the lattice parameters increases in the row: methanol < ethanol < butanol. The decrease of unit cell size *c*

is observed in the same order. The length/width ratio (*c*/*a*) for the resulting nanoparticles decreases with increasing hydrocarbon chain length in alcohols. The calculated nanoparticle crystallites have a size of 12 nm to 15 nm in width and 16 nm to 63 nm in length, which can also be observed in the images obtained by scanning electron microscopy. Also, increasing the chain length of hydrocarbon alcohols in the system shows an increase in the volume of the unit cell, which may indicate an increase in the amount of Ga^{3+} ions in the ZnO crystal lattice. Calculation of gallium content from solid X-ray photoelectron spectroscopy spectra revealed that the Ga^{3+} content is at least 2.06 % for the samples synthesized in methanol. In this case, a change in the amount of gallium in the $Zn_{0.9}Ga_{0.1}O$ samples synthesized in different media is also observed. The lowest concentration of gallium was observed in methanol synthesized ZnO samples, but the highest concentration was observed in butanal synthesized samples. The degree of doping varies from 2.06 % to 7.14 % in this case. This change in the gallium content is proportional to the changes observed in both the optical absorption/transmission spectra and band gap calculations.

3. Control of ZnO Charge Carriers by Photodoping

The gallium doped ZnO samples synthesized in methanol were subjected to photodoping (irradiated with UV radiation in hole-scavenging medium – *n*-butanol). Figure 10 (a) shows a visual representation of how the sample changes after photo-doping. Comparing X-ray diffraction patterns of the samples irradiated with UV light with those of the non-irradiated sample, no changes are observed (Fig. 10 (b)). Photodoped samples also continue to contain the crystalline phase of the wurtzite structure after UV treatment.

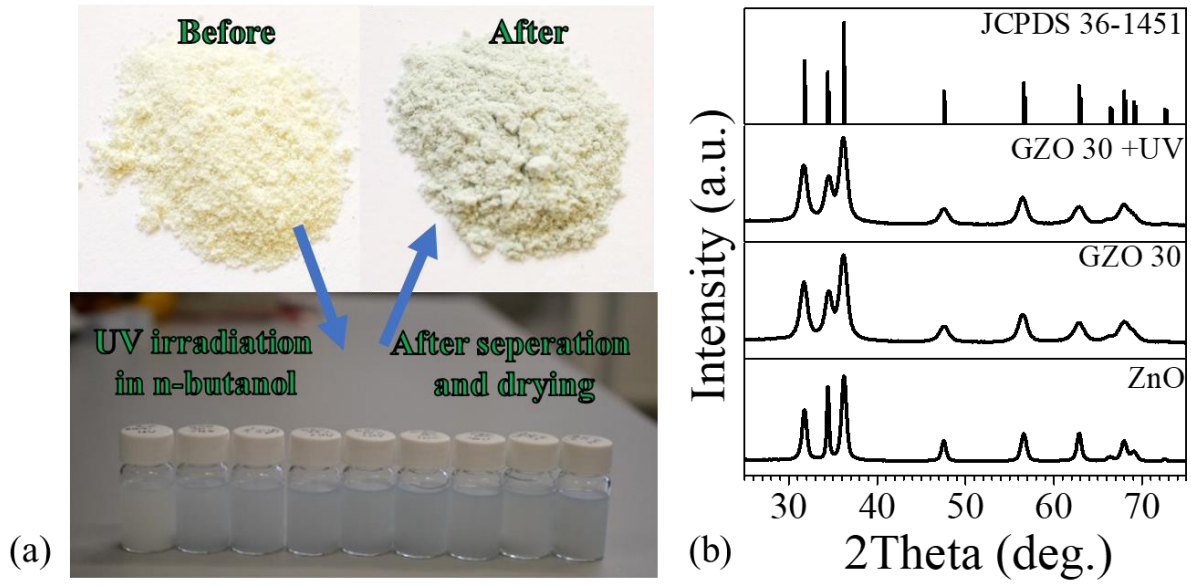

Fig. 10. GZO nanoparticle photo-doping: (a) GZO pre- and post-UV treatment and (b) X-ray diffraction patterns for the GZO 30 sample before and after photo-doping in the hole-scavenging medium.

The Rietveld refinement and XPS studies summarized in Table 3 show a comparison between the synthesized and photodoped GZO 30 samples. The content of gallium in the samples has practically not changed (these minor changes in the contents of gallium are within error). The crystallite size does not differ significantly between the irradiated and the non-irradiated samples. The small changes could be attributed to the uneven distribution of particle size. The microstrain for irradiated and non-irradiated samples is very similar.

Table 3

Summary of the Rietveld Refinement and Calculations of X-Ray Photoelectron Spectroscopy for ZnO Nanocrystals Doped With 30 mol % Gallium

Nominal Ga amount, mol %	**Crystallite sizes**		**Micro strains** $\sqrt{k2}$	**Metal ion ratio**		**Doping efficiency, %**
	***d*(100), nm**	***d*(001), nm**		**Ga, %**	**Zn, %**	
30	13.52 ± 0.16	19.60 ± 0.35	0.0087	7.0	93.0	23.33
30 + UV	14.81 ± 0.20	19.85 ± 0.39	0.0092	6.9	93.1	23.00

Examination of the particles by TEM (Fig. 11) shows that the overall size and shape of the particles before and after UV treatment has not changed. The irradiated and non-irradiated particles are crystalline and have a size less than 10–15nm.

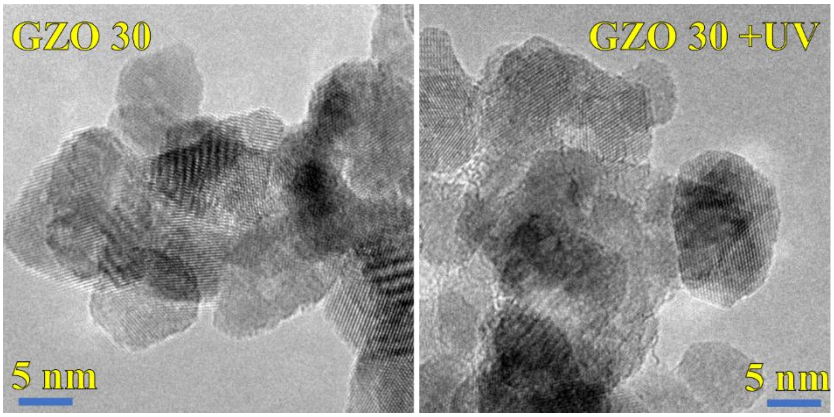

Fig. 11. TEM image of GZO 30 samples before and after UV treatment with *n*-butanol at higher magnifications.

The UV light irradiation kinetics and changes in absorbance over time (Fig. 12 (a)) indicate that it takes 50–70 hours or the photodoping process in *n*-butanol to reach saturation. The integrated area of the absorption in 400–1500 nm region shows that the changes in absorbance are logarithmic, indicating that during photo-doping the kinetics of the process gradually decelerates to saturation or, in this case, photochemical equilibrium. From this logarithmic change, it is seen that at the beginning of the photodoping process (Fig. 12 (b)), atmospheric oxygen in the vessel and oxygen dissolved in butanol is consumed, which postpones the initiation of the photochemical process.

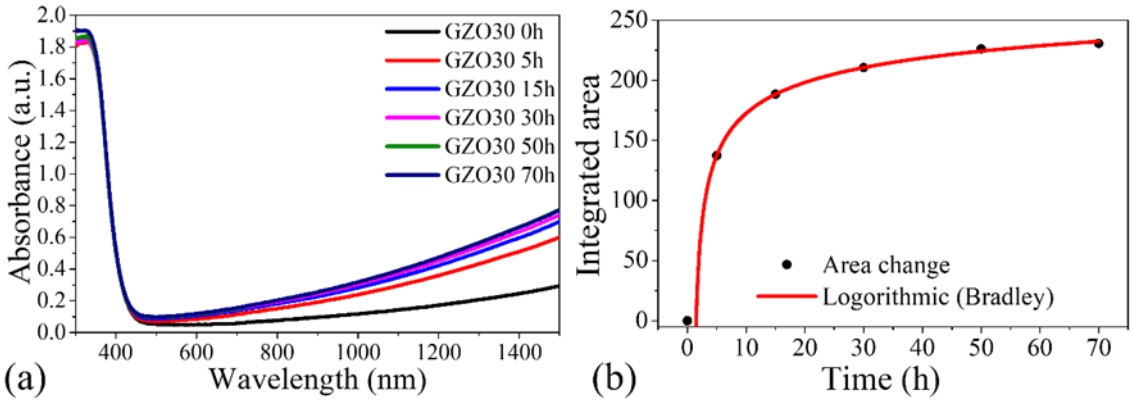

Fig. 12. Absorption kinetics of GZO samples: (a) change in absorbance over time of irradiation and (b) change in absorbance area (in the range of 450–1500 nm) over time.

The optical measurements of ZnO nanocrystals doped with 30 mol % of gallium are shown in Fig. 13. Measurements were carried out with dried samples before and after UV irradiation in a hole-scavenging medium (*n*-butanol). Measurements were also repeated 2 and 4 weeks after UV irradiation for the samples held in the air atmosphere. The optical absorption of the samples increases after UV irradiation in the range of about 400 nm to 1500 nm (Fig. 13). To quantify the increase in absorbance, the absorbance integral areas of each sample in the 400–1500 nm region before and after UV treatment were calculated. The obtained results reveal that UV irradiation in the hole-scavenging environment increases the absorption of infrared (IR) light. An increase in the absorption area ranging from 27 % to 58 % is observed for all samples in the 400–1500 nm region. The increase in light absorption in the infrared region can be attributed to the increase in the concentration of charge carriers in nanoparticles. To track the changes in IR light absorption for photodoped GZO nanoparticles, repeated light absorption measurements were performed in 2 and 4 weeks. It was found that after some time the absorbance in the range of 400–1500 nm slightly decreases (relaxation occurs) but is higher than the absorbance of the unirradiated sample, or reference sample. These results lead to the conclusion that ZnO doped with Ga has an independent stable photodoping effect in the environment. The additional positive charge introduced into the donor dopant crystal lattice can be compensated by various point defects, namely, electrons, zinc vacancies, or oxygen at the interstitial points according to Equations (2)–(4):

$$Ga_2O_3 \xrightarrow{ZnO} 2Ga_{Zn}^{\bullet} + 3O_O^X + V_{Zn}^{''}, \quad (2)$$

$$Ga_2O_3 \xrightarrow{ZnO} 2Ga_{Zn}^{\bullet} + 3O_O^X + O_i^{''}, \quad (3)$$

$$Ga_2O_3 \xrightarrow{ZnO} 2Ga_{Zn}^{\bullet} + 2O_O^X + \frac{1}{2}O_{2(g)} + 2e^{-}. \quad (4)$$

Only free electrons provide the desired optical properties. The observed permanent effect is related to electron compensation becoming the dominant compensation mechanism for Ga dopant charge as the result of photodoping.

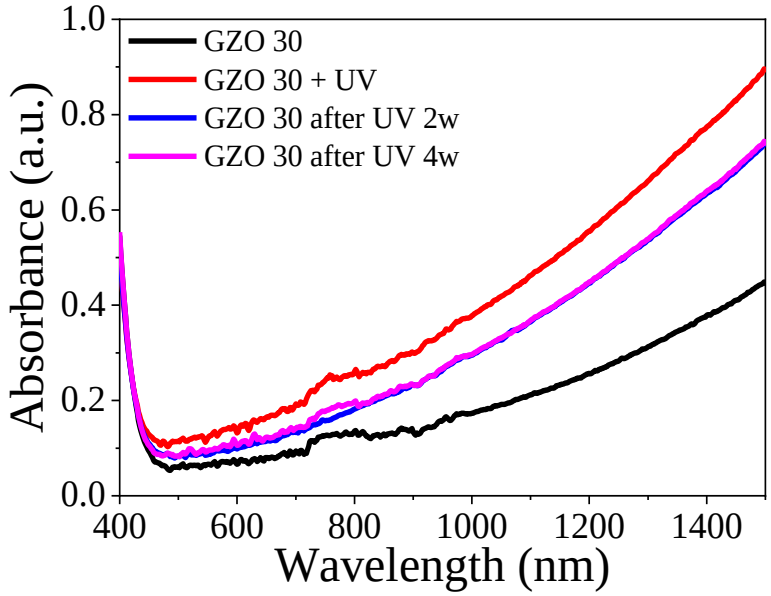

Fig. 13. 30 mol % Ga doped ZnO nanocrystal optical properties before and after UV irradiation, as well as in 2 and 4 weeks after UV irradiation.

To verify the possible modulation of the permanent photodoping effect, the photodoped nanocrystals were heated (oxidized) at 150 °C for 24 hours. After annealing, the nanocrystals were dispersed in a hole-scavenging medium and treated with UV light for a second time. The obtained absorption spectra are shown in Fig. 14 (a). During the heating at 150 °C, nanocrystals relax completely, but photodoping recovers the free electrons.

Photodoped materials also show the Burstein–Moss shift as revealed by optical band gap measurements (Fig. 14 (b)). The same shift is observed for the samples that have retained the photodoping effect for more than 4 weeks (Fig. 15 (a)). After treatment of particles at 150 °C, the band gap value decreases as expected (Fig. 15 (b)).

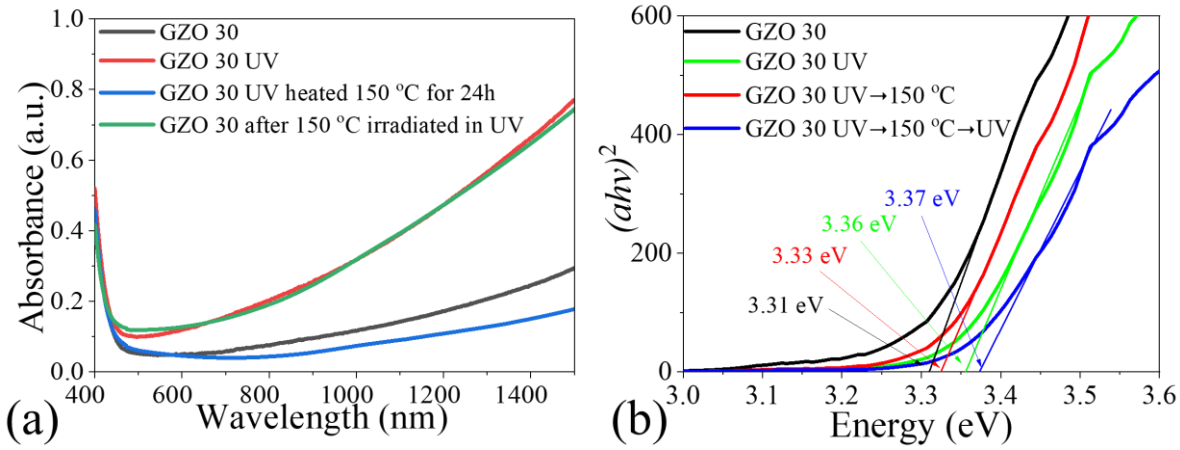

Fig. 14. ZnO nanocrystals doped with 30 mol % gallium: (a) absorption spectrum before and after UV treatment under different conditions and (b) representation of restricted zones.

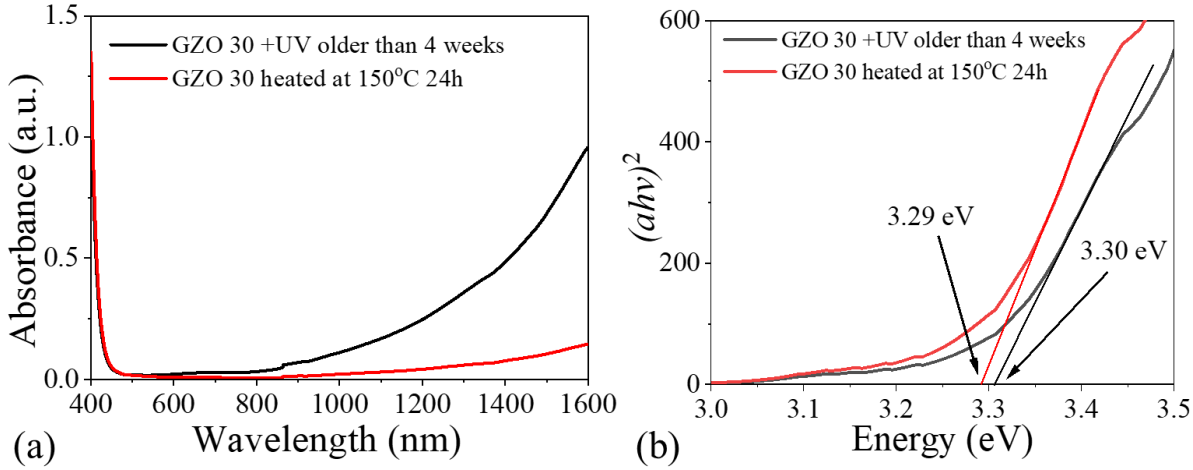

Fig. 15. ZnO nanocrystals doped with 30 mol % gallium 4 weeks after UV treatment: (a) absorption spectrum before and after heating at 150 °C and (b) representation of band gap.

ZnO samples with different doping levels were studied using photoluminescence spectroscopy (Fig. 16 (a) and (b)). The ZnO sample exhibits luminescence in the UV spectral region (360–400 nm). This part of the luminescence is attributed exciton recombination [9], [10]. In the visible part of the spectrum (400–550 nm) the samples doped with Ga show a broad emission region that indicates effects of defects on the doped ZnO nanocrystals (Fig. 10 (b)). After UV treatment, a decrease in the photoluminescence spectrum is observed due to the accumulation of free charge carriers in the conductivity region according to Auger recombination [7].

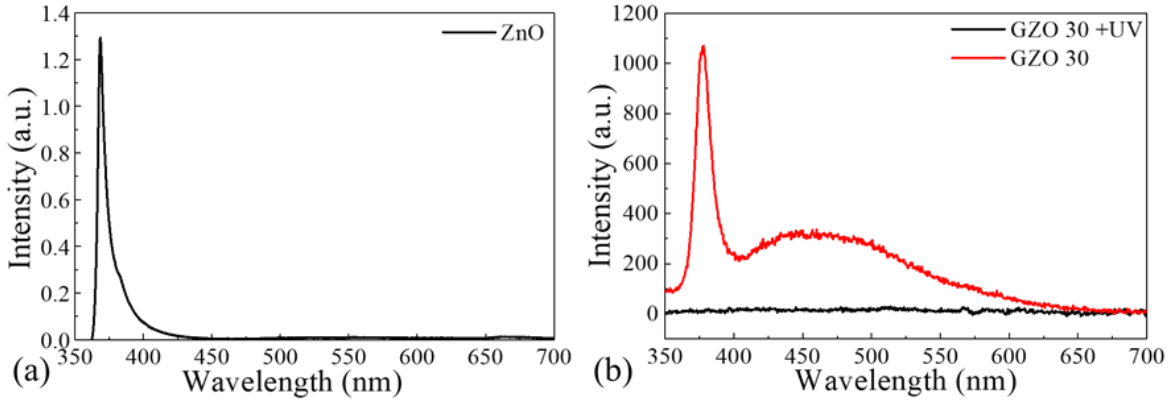

Fig. 16. Luminescence spectra of ZnO and Ga doped ZnO sample: (a) ZnO and (b) 30 mol % Ga doped ZnO (GZO 30) nanocrystals before and after UV treatment.

4. Transition Metal and Transition Metal-Gallium Co-Doped ZnO Diluted Magnetic Semiconductors

Synthesis of transition metal doped zinc oxide nanoparticles was performed by introducing iron, nickel, and manganese into the ZnO system. The concentration of these cations (Me = Ni, Fe, and Mn) was fixed at 5 mol % of total ZnO. The purpose of transition metal ion fixed concentration was to obtain diluted semiconductor magnets and to

demonstrate that the magnetic properties are controllable by the addition of delocalized electrons. From the X-ray diffraction patterns of the powder samples (Fig. 17 (a) and (b)) we can conclude that the dominating crystalline phase is wurtzite of zinc oxide (JCPDS 36-1451) with corresponding (*hkl*) diffraction plane peaks at 2θ = 31.8° (100), 34.5° (002), 36.3° (101), 47.6° (102) and 56.6° (110) (Fig. 17 (a) and (b)). In nickel-doped crystals, a peak located at 2θ = 44.7° related to metallic nickel impurity phase is observed in addition to the crystalline phase of wurtzite. This observed impurity phase at 2θ = 44.7° is deciphered as metallic nickel. Given that the sample shows only one small peak of this phase, its true composition is difficult to determine. Depending on added dopant, the diffraction peaks shift relative to the pure ZnO spectrum, since the transition metal ions introduced into the crystal lattice change the parameters of the lattice and promote the generation of strains.

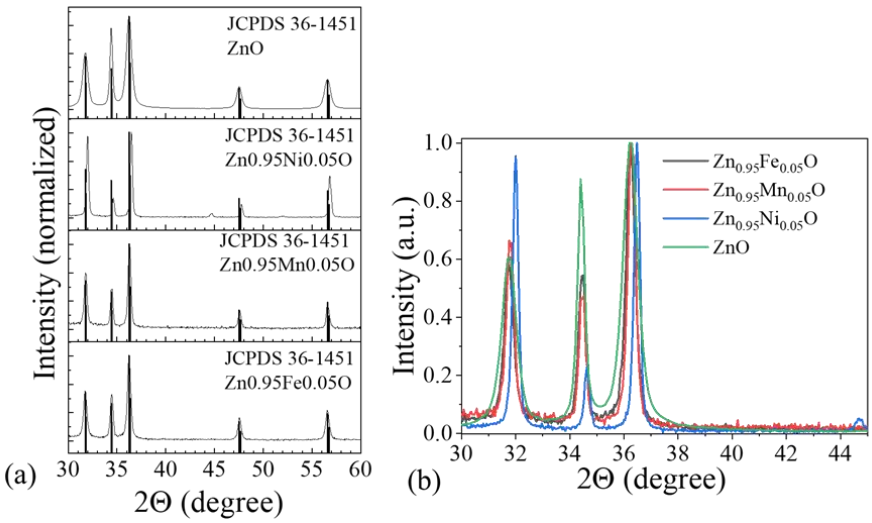

Fig. 17. X-ray diffraction pattern analysis of ZnO doped with 5 mol % various metal ions (a) overall image and (b) peak shift.

The results of SEM are shown in Fig. 18. As can be seen from these figures, during the solvothermal synthesis of ZnO there is a tendency to form nanorods with a length of 400–600 nm. The introduction of transition metals in the ZnO growth medium inhibits or promotes growth. In the presence of Fe ions, growth is hindered by the fact that the Fe and Zn ions exhibit the greatest difference in ion radius, leading to higher stresses in the crystals during growth. In the case of manganese and nickel, the difference in ionic radius is not that large, so the stress is not formed in the crystal. In the presence of nickel, particle growth also occurs in transverse direction. The presence of Ni ions disrupts the polarity of the growing planes of ZnO, improving the growth of the non-polar planes. ZnO growth during hydrothermal synthesis at elevated pH (≥12) is promoted by the formation of $Zn(OH)_4^{2-}$ and Na+ complex. Formation of the tetrahydroxy zincate ion is given in equation (5):

$$Zn(OH)_2 + 2(OH^-) \xrightarrow{pH \geq 12} Zn(OH)_4^{2-}. \quad (5)$$

This ion is responsible for the growth of ZnO polar planes [11]. The substitution of Zn ions with other valence ions (like Ga^{3+}) results in a surface charge change that inhibits

diffusion of tetrahydroxy zincate ions to the crystal surface. Due to equal charge repulsion, the growth of the (001) polar plane is reduced.

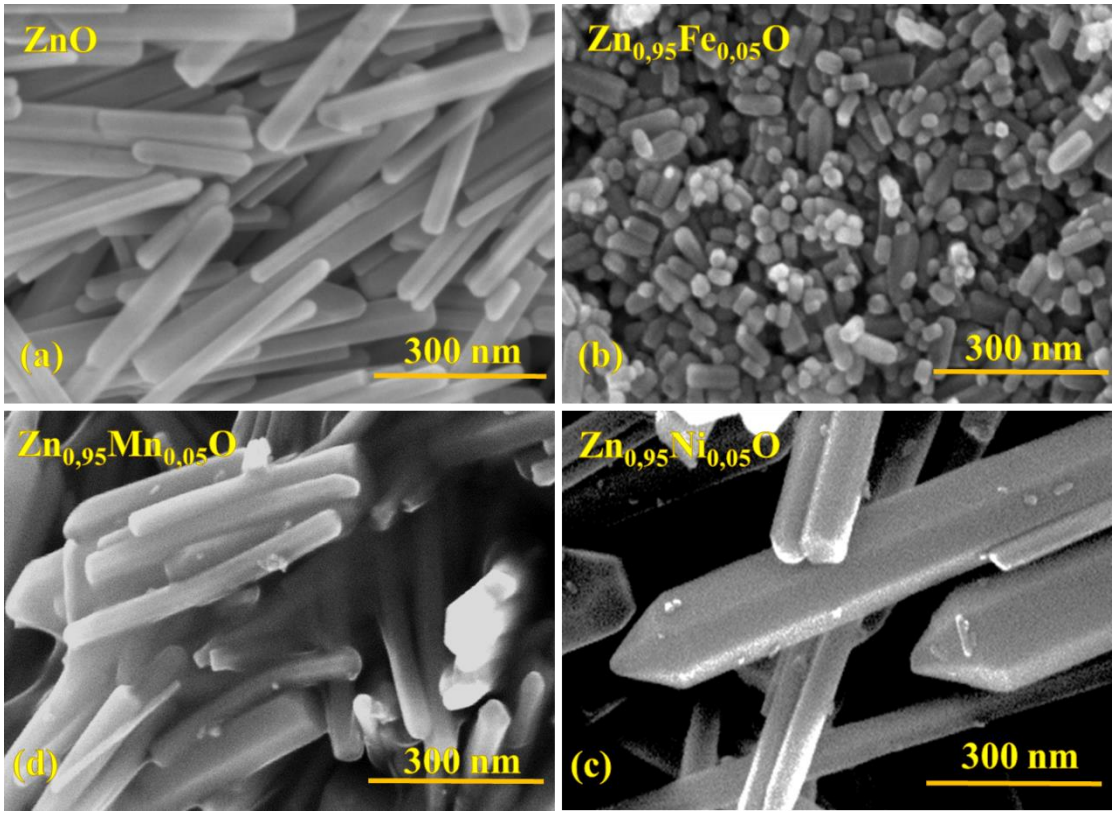

Fig. 18. Scanning electron microscopy images of the obtained $Zn_{0.95}Me_{0.05}O$ samples compared to a pure (a) ZnO sample synthesized in ethanol as well as ZnO samples doped with (b) Fe; (c) Mn and (d) Ni ions.

Rietveld refinement of the obtained X-ray diffraction patterns confirms the formation of wurtzite crystalline structures belonging to the $P6_3mc$ symmetry group in the samples under investigation. As already noted, the X-ray diffraction results of ZnO crystals doped with transition metals show changes in lattice parameters, which are shown in Table 5. Rietveld refinement indicates that the Fe, Ni, and Mn ions are present in ZnO structure. The addition of Fe and Mn increases the unit cell volume (V_0) of ZnO. The reason for this increased lattice volume could be the presence of larger high spin state Fe and Mn ions in the Zn lattice sites. This high spin state feature is confirmed in the literature and attributed to the formation of tetrahedral complexes [12]. The sizes of different ions are shown in Table 4. In the case of Ni ions, the lattice volume is smaller than that of pure ZnO.

Adding Ga^{3+} ions in the transition metal doped ZnO materials increase parameters *a* and *b* but decrease parameter c (increase *c*/*a* ratio). A decrease in this ratio is observed gradually with an increase in Ga^{3+} content.

Table 4

Results of Rietveld Refinement

Sample	Elementary cell parameters		*c*/*a*	V_0, Å^3	Micro strains $\sqrt{k2}$	Crystallite sizes		Goodness of fit *S*
	a, Å	*c*, Å				*d*(100) and *d*(010), nm	*d*(001), nm	
ZnO	3.2510	5.2076	1.6017	47.6211	0.0024	109 ± 10	212 ± 36	1.1589
$Zn_{0.95}Fe_{0.05}O$	3.2522	5.2021	1.5996	47.6487	0.0029	51.0 ± 2.1	117.0 ± 9.3	1.1374
$Zn_{0.925}Fe_{0.05}Ga_{0.025}O$	3.2520	5.2013	1.5994	47.6355	0.0034	40.0 ± 1.2	75.0 ± 3.5	1.2315
$Zn_{0.9}Fe_{0.05}Ga_{0.05}O$	3.2532	5.1905	1.5955	47.5717	0.0107	25.0 ± 1.4	67.0 ± 8.8	1.2441
$Zn_{0.875}Fe_{0.05}Ga_{0.075}O$	3.2530	5.1838	1.5935	47.5044	0.0122	15.0 ± 0.3	33.0 ± 1.6	1.2412
$Zn_{0.85}Fe_{0.05}Ga_{0.1}O$	3.2544	5.1882	1.5942	47.5857	0.0095	19.0 ± 0.7	33.0 ± 1.9	1.2503
$Zn_{0.95}Ni_{0.05}O$	3.2490	5.2071	1.6027	47.6007	0.0011	97.0 ± 4.0	258 ± 39	1.1228
$Zn_{0.925}Ni_{0.05}Ga_{0.025}O$	3.2528	5.2103	1.6018	47.7414	0.0046	45.0 ± 3.9	186 ± 53	1.8303
$Zn_{0.9}Ni_{0.05}Ga_{0.05}O$	3.2532	5.2094	1.6013	47.7449	0.0050	29.0 ± 1.1	69.0 ± 5.3	1.0989
$Zn_{0.875}Ni_{0.05}Ga_{0.075}O$	3.2524	5.2023	1.5995	47.6564	0.0082	18.0 ± 0.8	71.0 ± 9.9	1.1671
$Zn_{0.85}Ni_{0.05}Ga_{0.1}O$	3.2545	5.2046	1.5992	47.7391	0.0083	21.0 ± 1.1	63.0 ± 8.0	1.1760
$Zn_{0.95}Mn_{0.05}O$	3.2524	5.2090	1.6016	47.7178	0.0031	113 ± 12	226 ± 41	1.1303
$Zn_{0.925}Mn_{0.05}Ga_{0.025}O$	3.2528	5.2063	1.6006	47.7048	0.0040	38.0 ± 1.7	99.0 ± 9.4	1.4216
$Zn_{0.9}Mn_{0.05}Ga_{0.05}O$	3.2507	5.2055	1.6013	47.6359	0.0048	36.0 ± 1.2	122 ± 12	1.3183
$Zn_{0.875}Mn_{0.05}Ga_{0.075}O$	3.2528	5.1992	1.5984	47.6397	0.0097	36.0 ± 3.5	140 ± 45	1.1767
$Zn_{0.850}Mn_{0.05}Ga_{0.1}O$	3.2547	5.2027	1.5985	47.7275	0.0084	25.0 ± 1.1	69.0 ± 6.9	1.2959

The scanning electron microscopy studies concluded that the introduction of Ga^{3+} ions into $Zn_{0.95-x}Me_{0.05}Ga_xO$ systems inhibits the crystal growth as determined by Rietveld refinement. Figure 19 clearly shows that the crystal size along the *z*-axis has shrunk from several hundred nanometres to a few tens of nanometres in all sample systems. In systems containing Ni ions, a decrease along the *x* and *y* directions is also observed. This decline during the crystal growth is due to Coulomb repulsion, which is facilitated by free electrons that compensate Ga^{3+} ions at Zn^{2+} crystal lattice sites. This repulsion prevents the diffusion of zinc ions to the crystal surface, thus limiting lattice growth [11].

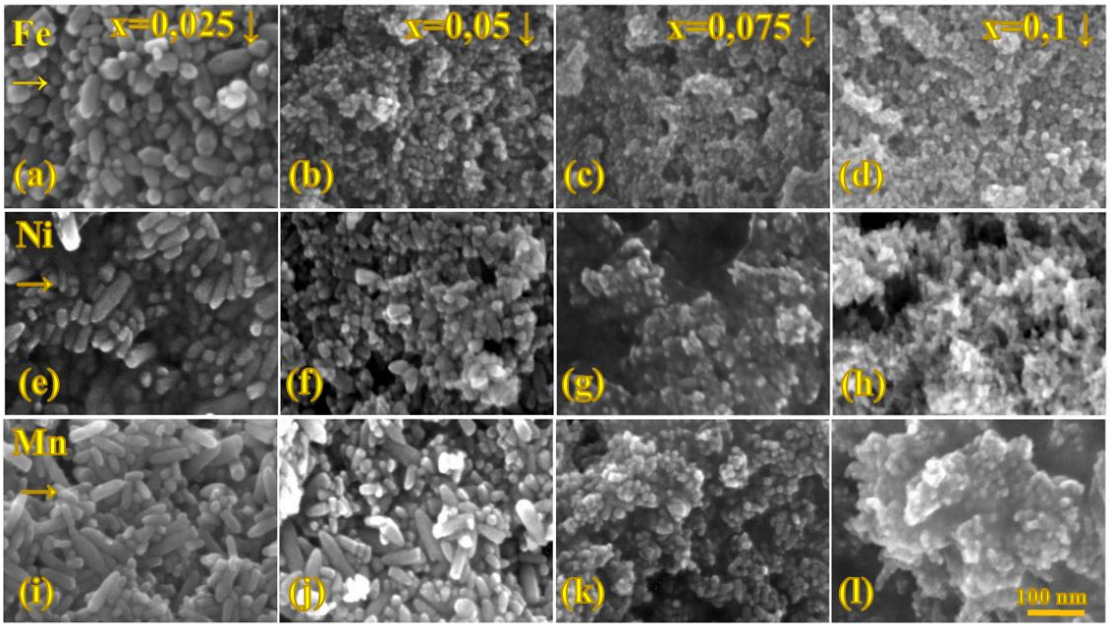

Fig. 19. Scanning electron microscopy images of $Zn_{0.95-x}Me_{0.05}Ga_xO$ system samples horizontally: (a)–(d) Me = Fe; (e)–(h) Me = Ni; (i)–(l) Me = Mn; and vertically depending on x = 0.025; 0.05; 0.075 and 0.1.

The magnetic properties at the room temperature and a summary of their parameters are shown in Fig. 20 and Table 5. Iron and nickel containing ZnO samples exhibit magnetic properties – ferromagnetic behaviour with hysteresis loop formation. This change has also been observed by other researchers with Fe doped ZnO nanocrystals [13]–[15] and Ni doped ZnO nanocrystals [16], [17]. Mn containing ZnO nanocrystals exhibit paramagnetic properties with no hysteresis loop.

The presence of gallium affects the magnetic properties. In the case of Fe containing samples, the magnetization decreases with increasing Ga^{3+} ions. The decrease in magnetization in this case could be due to the formation of crystal lattice defects, which lead to a weakening of the magnetization interaction. The change of magnetization by changing the concentration of Ga^{3+} ions is also observed in the samples containing Mn and Ni, but the nature of their change is not clear. As the samples containing Ni and Mn also contain crystalline phases of impurities, their effect on the total magnetic properties should be considered. Metallic nickel observed in X-ray analysis could be the main cause of ferromagnetic properties in nickel-containing specimens, and the increase in its amount alters the values of magnetization, coercive force and residual magnetization [18]. In the case of manganese, the individual Mn-containing crystalline phase could be the cause of the paramagnetic properties [19].

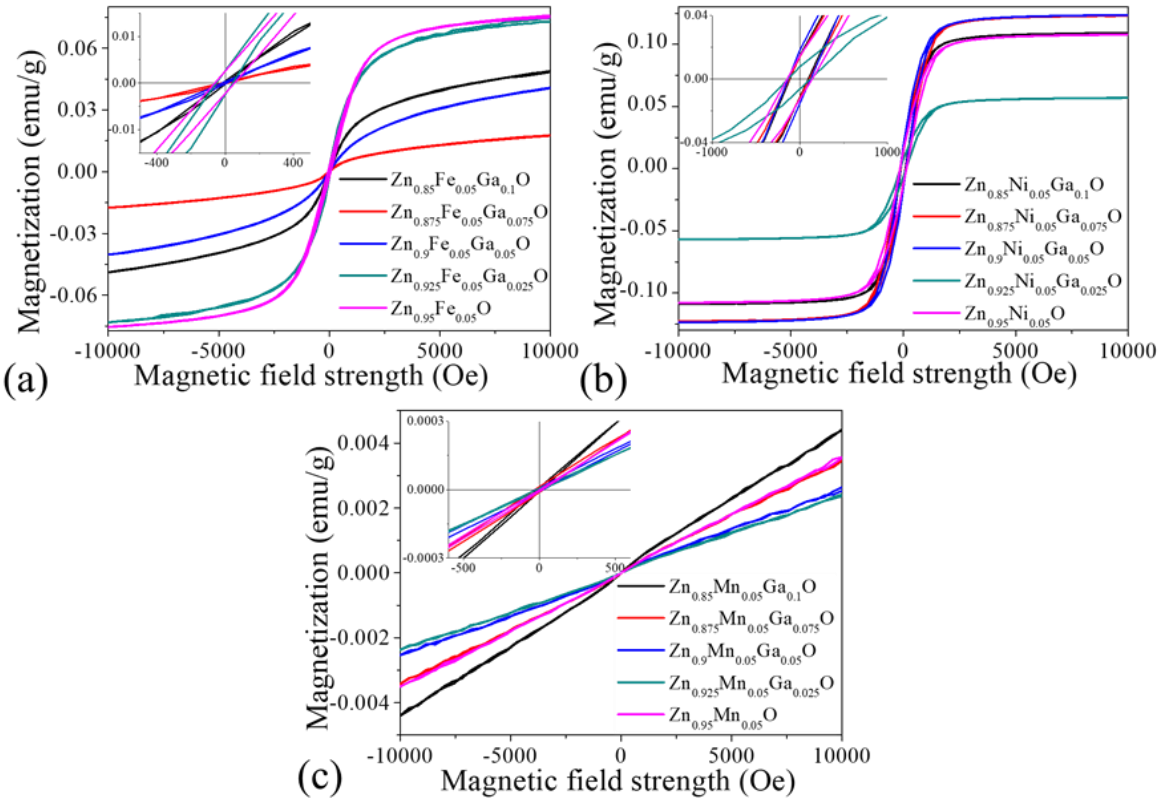

Fig. 20. Magnetization depending on magnetic field of $Zn_{0.95-x}Me_{0.05}Ga_xO$ samples: (a) Fe doped, (b) Ni doped, and (c) Mn doped samples.

Table 5

Summary of Magnetic Properties of the Obtained Samples

Sample	$M_{saturation}$, **emu · 10^{-3}**	H_C, **G**	M_g
$Zn_{0.95}Fe_{0.05}O$	75.667	57.840	0.00256
$Zn_{0.925}Fe_{0.05}Ga_{0.025}O$	73.852	47.388	0.00266
$Zn_{0.9}Fe_{0.05}Ga_{0.05}O$	40.553	13.017	0.00026
$Zn_{0.875}Fe_{0.05}Ga_{0.075}O$	17.638	19.106	0.00020
$Zn_{0.85}Fe_{0.05}Ga_{0.1}O$	48.897	11.223	0.00040
$Zn_{0.95}Ni_{0.05}O$	107.82	142.72	0.01451
$Zn_{0.925}Ni_{0.05}Ga_{0.025}O$	57.041	128.43	0.00764
$Zn_{0.9}Ni_{0.05}Ga_{0.05}O$	123.64	127.69	0.01803
$Zn_{0.875}Ni_{0.05}Ga_{0.075}O$	123.20	113.84	0.01384
$Zn_{0.85}Ni_{0.05}Ga_{0.1}O$	109.15	103.84	0.01483
$Zn_{0.95}Mn_{0.05}O$	3.5403	8.1759	$-7.42\cdot10^{-8}$
$Zn_{0.925}Mn_{0.05}Ga_{0.025}O$	2.3979	17.645	$7.59\cdot10^{-6}$
$Zn_{0.9}Mn_{0.05}Ga_{0.05}O$	2.5902	23.439	$8.25\cdot10^{-6}$
$Zn_{0.875}Mn_{0.05}Ga_{0.075}O$	3.4487	28.361	$1.39\cdot10^{-5}$
$Zn_{0.850}Mn_{0.05}Ga_{0.1}O$	4.4150	13.911	$9.80\cdot10^{-6}$

CONCLUSIONS

1. Using the solvothermal synthesis method, ZnO nanoparticles with different amount of gallium doping were obtained, concentration of which, depending on the initial nominal gallium concentration (0–30 mol %) in the synthesis, can be increased up to 7 %.
2. Increasing the nominal gallium concentration in the synthesis reduces the doping efficiency of ZnO from 80 % to 23 %.
3. During the synthesis at a fixed nominal amount of gallium of 10 mol % by providing more reducing synthesis conditions, it is possible to increase the doping efficiency from 20 % to 70 %.
4. When doping ZnO with gallium, nanocrystals begin to absorb light in the infrared part of the spectrum, increase the band gap due to the Moss–Burstein effect, decrease exciton luminescence and shift in the fundamental mode of E_{1L} in Raman spectra, indicating the presence of delocalized electrons in the conduction region.
5. Using photodoping, it is possible to increase the concentration of delocalized charge carriers in Ga-ZnO nanocrystals, which can be observed with the expansion of the band gap due to Burstein–Moss shift as well as higher absorption in the infrared part of the spectrum.
6. Depending on the introduced transition metal ion, the magnetic interaction in ZnO nanocrystals changes. The introduction of iron and nickel ZnO causes ferromagnetic properties, while the introduction of manganese causes paramagnetic properties.
7. By changing the concentration of gallium in zinc oxide nanocrystals doped with transition metals, a change in magnetic interaction is observed, which is related to the presence of gallium and its defects in the crystals.
8. The obtained Ga-ZnO nanocrystals, due to their infrared light absorption, could be used in the creation of smart windows for temperature control in buildings.
9. The acquired knowledge about magnetic semiconductor oxide nanocrystals and their changing magnetic properties will provide important information in the field of material design for the manufacture of various magnetic devices.

REFERENCES

[1] I. Kriegel, F. Scotognella, and L. Manna, "Plasmonic doped semiconductor nanocrystals: Properties, fabrication, applications and perspectives," *Phys. Rep.*, vol. 674, pp. 1–52, 2017.

[2] T. Kataoka *et al.*, "Electronic structure and magnetism of the diluted magnetic semiconductor Fe-doped ZnO nanoparticles," *J. Appl. Phys.*, vol. 107, no. 3, pp. 1–7, 2010.

[3] F. Scotognella *et al.*, "Plasmonics in heavily-doped semiconductor nanocrystals Francesco," *Eur. Phys. J. B*, vol. 86, no. 154, pp. 1–21, 2013.

[4] I. Gryczynski *et al.*, "Surface-plasmon-coupled emission of quantum dots.," *J. Phys. Chem. B*, vol. 109, no. 1, pp. 1088–1093, 2005.

[5] Y. E. Kesim, E. Battal, and A. K. Okyay, "Plasmonic materials based on ZnO films and their potential for developing broadband middle-infrared absorbers," *AIP Adv.*, vol. 4, no. 7, pp. 1–8, 2014.

[6] C. Dhand *et al.*, "Methods and strategies for the synthesis of diverse nanoparticles and their applications: A comprehensive overview," *RSC Adv.*, vol. 5, no. 127, pp. 105003–105037, 2015.

[7] A. Agrawal, S. H. Cho, O. Zandi, S. Ghosh, R. W. Johns, and D. J. Milliron, "Localized Surface Plasmon Resonance in Semiconductor Nanocrystals," *Chem. Rev.*, vol. 118, no. 6, pp. 3121–3207, 2018.

[8] A. M. Schimpf, C. E. Gunthardt, J. D. Rinehart, J. M. Mayer, and D. R. Gamelin, "Controlling carrier densities in photochemically reduced colloidal ZnO nanocrystals: Size dependence and role of the hole quencher," *J. Am. Chem. Soc.*, vol. 135, no. 44, pp. 16569–16577, 2013.

[9] M. Saha, S. Ghosh, V. D. Ashok, and S. K. De, "Carrier concentration dependent optical and electrical properties of Ga doped ZnO hexagonal nanocrystals," *Phys. Chem. Chem. Phys.*, vol. 17, no. 24, pp. 16067–16079, 2015.

[10] W. Zhu *et al.*, "Analysis of defect luminescence in Ga-doped ZnO nanoparticles," *Phys. Chem. Chem. Phys.*, vol. 18, no. 14, pp. 9586–9593, 2016.

[11] R. Chen, P. Zhu, L. Deng, T. Zhao, R. Sun, and C. Wong, "Effect of aluminum doping on the growth and optical and electrical properties of ZnO nanorods," *Chempluschem*, vol. 79, no. 5, pp. 743–750, 2014.

[12] S. Livingstone, "A Review of: "The Early Transition Metals," *Synth. Inorg. Met. Chem.*, vol. 3, no. 4, pp. 423–424, 1973.

[13] M. Fang, W. Voit, A. Kyndiah, Y. Wu, L. Belova, and K. V. Rao, "Room temperature ferromagnetism of Fe-doped ZnO and MgO thin films prepared by ink-jet printing," *MRS Proc.*, vol. 1394, pp. 1–8, 2012.

[14] F. Wang, W. W. Huang, S. Y. Li, A. Q. Lian, X. T. Zhang, and W. Cao, "The magnetic properties of $Fe_xZn_{1-x}O$ synthesized via the solid-state reaction route: Experiment and theory," *J. Magn. Magn. Mater.*, vol. 340, pp. 5–9, 2013.

[15] M. V. Limaye, S. B. Singh, R. Das, P. Poddar, and S. K. Kulkarni, “Room temperature ferromagnetism in undoped and Fe doped ZnO nanorods: Microwave-assisted synthesis,” *J. Solid State Chem.*, vol. 184, no. 2, pp. 391–400, 2011.

[16] S. Fabbiyola, V. Sailaja, L. J. Kennedy, M. Bououdina, and J. Judith Vijaya, “Optical and magnetic properties of Ni-doped ZnO nanoparticles,” *J. Alloys Compd.*, vol. 694, pp. 522–531, 2017.

[17] A. Samanta, M. N. Goswami, and P. K. Mahapatra, “Magnetic and electric properties of Ni-doped ZnO nanoparticles exhibit diluted magnetic semiconductor in nature,” *J. Alloys Compd.*, vol. 730, pp. 399–407, 2018.

[18] H. Liu *et al.*, “Role of point defects in room-temperature ferromagnetism of Cr-doped ZnO,” *Appl. Phys. Lett.*, vol. 91, no. 072511, pp. 1–4, 2007.

[19] A. Goktas, I. H. Mutlu, Y. Yamada, and E. Celik, “Influence of pH on the structural optical and magnetic properties of $Zn_{1-x}Mn_xO$ thin films grown by sol-gel method,” *J. Alloys Compd.*, vol. 553, pp. 259–266, 2013.